https://doi.org/10.5194/egusphere-2024-1560
Preprint. Discussion started: 4 June 2024

Water Vapor Content Retrieval Under Cloudy Sky Conditions From SWIR Satellite Measurements in the Context of C^{3}IEL Space Mission Project

Raphaël Peroni[1], Céline Cornet[1], Olivier Pujol[1], Guillaume Penide[1], Clémence Pierangelo[2], and François Thieuleux[1]

[1]Univ. Lille, CNRS, UMR 8518 - LOA - Laboratoire d'Optique Atmosphérique, F-59000 Lille, France
[2]Centre National d'Etudes Spatiales (CNES), 18 avenue Edouard Belin, 31401 TOULOUSE Cedex 9, France

Correspondence: Céline Cornet (celine.cornet@univ-lille.fr)

Abstract. A retrieval algorithm of integrated water vapor content above cloud, using shortwave infrared observations, is developed and evaluated through idealized and realistic atmospheric profiles. Water vapor plays a crucial role in cloud formation and development, particularly those resulting from convective processes. They influence locally the spatiotemporal variability of atmospheric water vapor content, through exchanges between clouds and their immediate environment. Therefore, a better understanding of water vapor content above and around cloud is necessary to improve our comprehension of interactions between water vapor and cloud to better constrain Large-Eddy Simulation and numerical weather forecasting models. The developed algorithm is part of the Cluster for Cloud evolution, ClImatE and Lightning, C^{3}IEL space mission project. This mission, scheduled for 2027 aims to enhance our knowledge of the 3D convective cloud development velocities, the electrical activity associated with convective systems and the water vapor content above and around cloud. The retrieval algorithm presented in this study was achieved through a Bayesian probabilistic approach, the optimal estimation method. The atmosphere was assumed to be composed of homogeneous plane-parallel layers, and synthetic radiance datasets were generated for testing the developed retrieval algorithm. The feasibility of retrieving integrated water vapor content above cloud and over the ocean from SWIR radiances was shown to have a precision of approximately $1\ \mathrm{kg.m^{-2}}$ for optically thick clouds under idealized cloudy sky conditions. Tests using realistic water vapor and cloud extinction profiles that present non-homogeneous vertical distributions show that integrated water vapor content above low/mid-level clouds could be retrieved with a positive bias related to cloud vertical penetration of approximately $2.6\ \mathrm{kg.m^{-2}}$. The algorithm fails for very low water vapor content encountered in the presence of high deep convective clouds.

1 Introduction

Clouds play a significant role in the Earth energy balance, as they can induce a positive or negative radiative forcing whose uncertainty is still important, (*e.g.,* Stocker et al., 2013; Masson-Delmotte et al., 2021). Depending on their latitude, characteristics, altitude and temperature, their radiative forcing can be different (*e.g.,* Ramanathan et al., 1989; Harrison et al., 1990). Indeed, lower tropospheric clouds, which are primarily composed of liquid water, tend to reflect solar radiation at all

https://doi.org/10.5194/egusphere-2024-1560
Preprint. Discussion started: 4 June 2024

wavelengths, resulting in cooling effect (*e.g.,* Fermepin and Bony, 2014), named parasol effect (*e.g.,* Crutzen and Ramanathan, 2003). On the contrary, upper tropospheric clouds such as *cirrus* or deep convective clouds, tend to absorb thermal radiation from the Earth and re-emit infrared radiation towards space at a lower temperature corresponding to a lower energy, thus resulting in the greenhouse effect (*e.g.,* Jensen et al., 1996; McFarquhar et al., 2000; Lee et al., 2009; Schmidt et al., 2010).

It is therefore essential to better understand cloud development in order to accurately assess their radiative impact on the Earth's energy balance. As an example, Bony et al. (2015) address the scientific community with several questions aimed at emphasizing the importance of a better understanding of the role of cloud feedbacks and convective organization on climate, as well as the factors that influence cloud formation.

Cloud formation and development depend on the amount of water vapor available in the atmosphere. Indeed, with regard to the temperature, the saturation vapor pressure can be reached. Water vapor will then condense either on Cloud Condensation Nuclei (CCN) to form new cloud droplets or on Ice Nuclei (IN), to form new ice crystals. The latent heat released during water vapor condensation and cloud formation not only disturbs the thermal structure of the atmosphere (*e.g.,* Trenberth and Smith, 2005; Schneider et al., 2010) but also fuels cloud development through a chain reaction.

In the free troposphere, humidity influences the dynamic development of clouds through entrainment and detrainment processes. Convection processes, in return, contribute significantly to the redistribution of energy and water vapor in the atmosphere (*e.g.,* Blyth, 1993). Humidity above and around clouds is therefore an essential parameter in the process of cloud development, particularly in the case of convective clouds.

Many spaceborne remote sensing instruments have been developed to retrieve water vapor across various spectral domains. Microwave sounders such as SAPHIR aboard the French-Indian satellite MEGHA-TROPIQUES (*e.g.,* Desbois et al., 2007), or AMSU-A/AMSU-B, make it possible to conduct measurements at all weather conditions and provide either humidity profiles or information on total water vapor content at a spatial resolution of $12\ \mathrm{km}$ at nadir for SAPHIR (*e.g.,* Rao et al., 2013), 48 km at nadir for AMSU-A, and 16 km for AMSU-B (*e.g.,* Rosenkranz, 2001; Karbou et al., 2005). Humidity profile retrieval in clear sky conditions or above thick clouds are also performed by IASI instrument operating in the thermal infrared (TIR) with a spatial resolution of $8\ \mathrm{km}$ (*e.g.,* Schlüssel and Goldberg, 2002; Hilton et al., 2012). The limitation of these instruments to study cloud and water vapor interactions lies in their low spatial resolutions and not contiguous pixels, which do not allow for precise examination of these interactions.

Near-Infrared (NIR) or Shortwave Infrared (SWIR) imagers allow to derive water vapor content at a better spatial resolution under clear sky conditions through the differential absorption method, either with airborne measurements (*e.g.,* Bouffiès et al., 1997), or from spaceborne sensors such as POLDER (*e.g.,* Vesperini et al., 1999), MERIS (*e.g.,* Bennartz and Fischer, 2001) or ENVISAT and MODIS (*e.g.,* Gao and Kaufman, 2003). All of these retrieval algorithms propose parameterizations that link the Integrated Water Vapor Content, in $\mathrm{kg.m^{-2}}$, to the ratio of NIR or SWIR spectral bands within absorbing and non-absorbing channels. However, in cloudy sky conditions, these parameterizations are no longer sufficient as clouds interfere with the measurements. Indeed, in this particular spectral domain, clouds are not transparent to radiation (as it is in the microwave domain). Moreover, as they do not act as a perfect reflector radiation penetrate the cloud and get scattered. It effectively extends the radiation's path through the atmosphere and consequently increasing absorption by water vapor. Albert et al.

https://doi.org/10.5194/egusphere-2024-1560
Preprint. Discussion started: 4 June 2024

(2001) demonstrates the feasibility of retrieving water vapor content above cloud in the SWIR domain, over various types of surface, and in the presence of low and optically thick clouds, applying the differential absorption method to simulations conducted in the context of the POLDER and MERIS instruments. They demonstrated with simulations that the absorption of solar radiation within a water vapor absorption band is influenced by the "radiation path", modified by the presence of clouds. On one hand, multiple scattering increases the path length traveled by radiation, leading to higher absorption by water vapor and consequently, a higher retrieved water vapor content. On the other hand, the presence of clouds reduces or stops the influence of lower atmospheric layers, resulting in reduced overall absorption (Albert et al., 2001).

In this study, the objective is to obtain information on the integrated water vapor content above cloud using SWIR satellite observations with high spatial and temporal resolution over the ocean by accounting for the cloud top position and the scattering within the cloud. Firstly, in section 2, we provide an overview of the study's context, specifically the space mission project that contextualizes our work. Then in section 3, we discuss the method employed in the developed retrieval algorithm. Section 4 shows the sensitivity of the C^{3}IEL channels to the $IWVAC$. In section 5, the algorithm is tested first under idealized cloudy atmospheric conditions, and under realistic conditions. Finally, section 6 summarizes the main findings.

2 The C^{3}IEL space mission project

The space mission project named as the Cluster for Cloud evolution, ClImatE and Lightning, C^{3}IEL (Rosenfeld et al., 2022) has been initiated in 2016 through a partnership between the French space agency (CNES) and the Israeli Space Agency (ISA). Its primary objective is to explore the dynamical development of convective clouds, including *cumulus congestus* and *cumulonimbus* clouds. This will be achieved by gathering data at high spatial and temporal resolutions, through 11 acquisitions of two simultaneous observations every 20 seconds. C^{3}IEL will consist of a pair of satellites operating in tandem, distanced by about 150 km following a sun-synchronous orbit at about 1 : 30 PM local time at the equator. The altitude of the orbit is expecting to be between 600 and 700 km. The underlying measurement principles is represented in figure 1. This strategy of observations will provide (1) the 3D envelope of convective clouds and their vertical/horizontal development velocities (Dandini et al., 2022) using the visible imagers named CLOUD, measuring at 670 nm with a high spatial resolution (20 m at nadir), (2) the associated electrical activity generated by convective processes with the instruments Lightning Optical Imager and Photometers (LOIP) consisting in visible imagers measuring at 777 nm with a spatial resolution of 140 m at nadir and two photometers at 337 and 777 nm and (3) the water vapor content above and around convective clouds using the three shortwave infrared (SWIR) imagers, with a spatial resolution of 125 m at nadir.

This paper focuses on the development of a retrieval algorithm for the Integrated Water Vapor content Above Cloud ($IWVAC$) retrieval from three SWIR water vapor imagers on each satellite. Figure 2 shows the water vapor transmission spectrum in this spectral range and the three spectral bands selected for the C^{3}IEL water vapor imagers. The first band (1) is a non-absorbing band centered at 1.04 µm; the second band (2) is a moderately absorbing band centered at 1.13 µm; the third one is a highly absorbing band centered at 1.37 µm. The three bands will have a spectral width of about 0.02 µm.

https://doi.org/10.5194/egusphere-2024-1560
Preprint. Discussion started: 4 June 2024

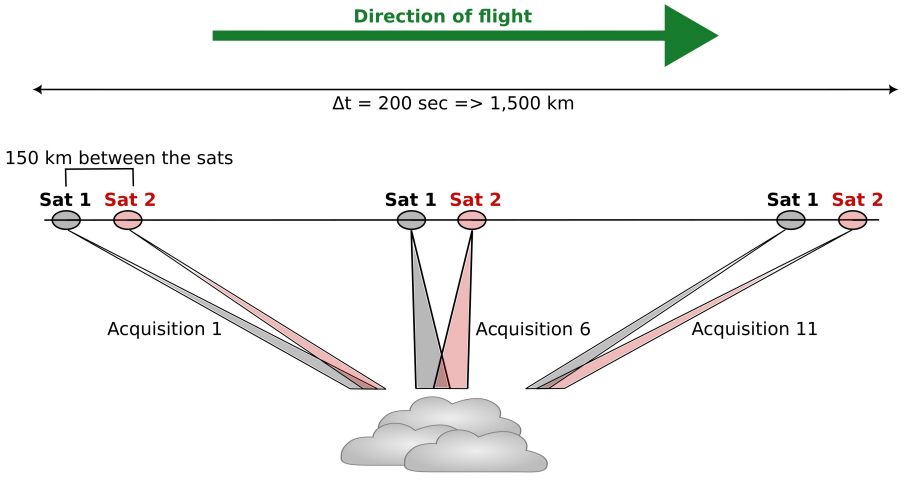

Figure 1. Illustration of the principle of the Cluster for Cloud evolution, ClImatE and Lightning (C^3IEL), observations.

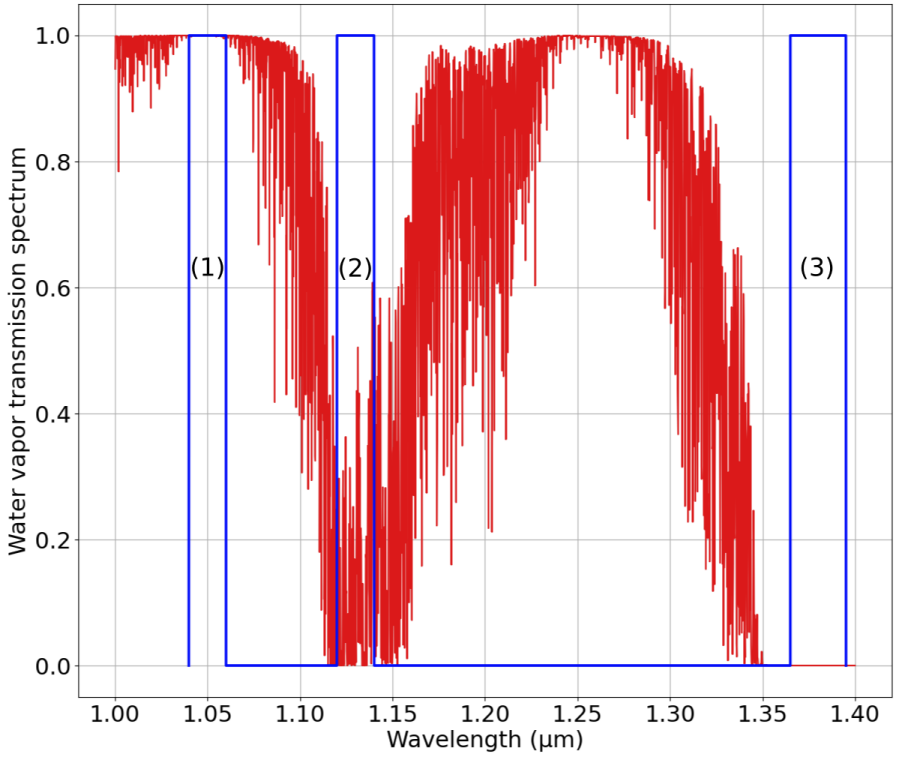

Figure 2. Water vapor transmission spectrum in clear sky condition at nadir (red curve) and the three SWIR spectral bands for the study of water vapor in the context of the C^3IEL space mission (blue rectangles).

https://doi.org/10.5194/egusphere-2024-1560
Preprint. Discussion started: 4 June 2024

3 Description of the methodology

This section introduces the retrieval scheme used in our study. It follows an Optimal Estimation Method (OEM) scheme (Rodgers, 2000), with the aim to get the 1D equivalent Cloud Optical Thickness (COT) and the Integrated Water Vapor Above Cloud ($IWVAC$). The OEM is a Bayesian statistical approach commonly used in remote sensing in order to estimate atmospheric and surface properties from measurements, such as satellite remote sensing (*e.g.,* Sourdeval et al., 2013, 2015; Leonarski et al., 2020; Matar et al., 2023). The objective of the OEM is to minimize the difference between the measured and the simulated radiance, under the constraint of *a priori* knowledge about the atmosphere. Equation (1) formalizes how the OEM works:

$$y = F(x, b) + \epsilon \tag{1}$$

where the vector y contains the measured radiances and F denotes the forward model including the model assumed for the retrieval and the radiative transfer code to get radiances from atmospheric properties. The state vector (x) contains the parameters to retrieve (see section 3.1), whereas b specifies the fixed parameters within the forward model (see section 3.2). Lastly, the vector ϵ contains the errors assumed to be randomly distributed, encompassing measurement uncertainties, errors in the fixed parameters and related to the forward model. Because forward model errors are extremely hard to estimate properly, as usually done, only uncertainties associated with measurements and fixed parameters are considered in this paper.

3.1 Measurement and state vectors: y and x

Water vapor retrieval in the context of the C^{3}IEL space mission is based on the exploitation of three spectral bands in the SWIR. The non-absorbing one (centered at 1.04 µm) will be sensitive to the 1D equivalent COT, while the two other bands (centered at 1.13 and 1.37 µm) will serve to retrieve the $IWVAC$.

The measurement vector contains thus the radiance values measured in the three spectral bands described above:

$$y = \begin{bmatrix} R_{1.04} \\ R_{1.13} \\ R_{1.37} \end{bmatrix} \tag{2}$$

As the C^{3}IEL mission is still not in orbit, these radiances are simulated to develop and evaluate the algorithm using atmospheric and cloud profiles described in section 5. Measurement vector data will be associated with an uncertainty of 5 %.

The state vector contains the desired parameters, COT and $IWVAC$:

$$x = \begin{bmatrix} \text{COT} \\ \text{IWV AC} \end{bmatrix} \tag{3}$$

The uncertainty on the *a priori* knowledge is arbitrarily set to $10,000$ %, in order to minimize its influence and give more weight to the measurements during the retrieval process.

https://doi.org/10.5194/egusphere-2024-1560
Preprint. Discussion started: 4 June 2024

At the end of the OEM process, the variance-covariance matrix of the retrieved state vector can be computed and gives the uncertainties on the retrieved parameters (*a posteriori* uncertainties, noted σ_x) with the following relationship (Rodgers, 2000):

$$\sigma_x = \sqrt{\left(S_a^{-1} + K_i^T S_\epsilon^{-1} K_i\right)^{-1}} \tag{4}$$

which is the square root of the *a posteriori* variance-covariance matrix. In this expression, S_a is the *a priori* variance-covariance matrix, K the jacobian, and S_ϵ the error variance-covariance matrix associated with the measurements and fixed parameters (see Appendix A for more details).

3.2 Fixed parameters: b

The cloud model defined in the developed retrieval algorithm assumes a 1D homogeneous plane-parallel layer between the Cloud Base Height (CBH) and its top altitude (CTH), horizontally infinite over the ocean. Table 1 describes the fixed parameters used in the developed retrieval algorithm and their uncertainties.

Table 1. Description of the fixed parameters and their uncertainties.

Fixed parameter (b)	Value	Uncertainty (ϵ_b)
Surface albedo	0.060	$\pm$0.006
Cloud Base Height (CBH)	0.2 km	$\pm$ 0.1 km
Cloud Top Height (CTH)	provided by C^{3}IEL visible imager	$\pm$ 0.04 km
Droplet [Ice] effective radius	10 [45] µm	$\pm$ 5 µm

In this study, we consistently assign a surface albedo of 0.060, representing an ocean surface, with an uncertainty chosen to be 10 %. The CTH varies based on the atmospheric profile used to simulate the measurements (detailed in section 5.2.1). In practice, it will be determined by combining data from the pair of visible imagers designed for studying the 3D envelope and development velocities. The CTH uncertainty is set to 0.04 km (Dandini et al., 2022). The effective radius of cloud droplets is fixed at an average value of 10 µm (*e.g.,* King et al., 2004), with an accuracy of 50 %. The effective radius of ice crystals is set to an average value of 45 µm with an associated uncertainty of 5 µm. These values represent the mean and standard deviation of the ice effective radius calculated using the Wyser parameterization (Wyser, 1998) applied on the whole database described in section 5.2.1.

3.3 Radiative transfer model: F

Our study combined an OEM method with the radiative transfer code ARTDECO (Atmospheric Radiative Transfer Database for Earth and Climate Observation) in order to solve the Radiative Transfer Equation (RTE) by means of the adding-doubling model (de Haan et al., 1987). ARTDECO (https://www.icare.univ-lille.fr/artdeco/, Dubuisson et al., 2016) is a tool that gathers various models and data used to simulate Earth total and polarized atmosphere radiances and radiative fluxes, from the UV to

https://doi.org/10.5194/egusphere-2024-1560
Preprint. Discussion started: 4 June 2024

the thermal IR range (200 nm to 50 µm). It uses the homogeneous plane-parallel approximation and permits to compute some aerosols and clouds optical properties.

3.4 IWV AC retrieval: principle and assumptions

As the measurements contain limited information on the atmospheric profile, some assumptions are needed to constrain the model.

1. Molecular Rayleigh scattering not considered since it is negligible in the SWIR
2. Relative Humidity (RH) equal to 100 % within the cloud
3. Cloud Base Height (CBH) fixed at 0.2 km corresponding to the average minus the standard deviation value calculated from the ECMWF-IFS profiles described in section 5.2.1

As explained above, the main objective of the developed retrieval algorithm is to minimize the difference between the measured radiances and the radiances simulated by the forward model. The process begins with a first guess value for the state vector including the 1D equivalent COT and $IWVAC$. In each iteration, the state vector is adjusted to achieve simulated radiances closer to the measured one. The COT, being an input parameter in the radiative transfer code, is subject to a direct adjustment at each iteration. The $IWVAC$ follows a different approach as it represents the vertical integration of the water profile above cloud used in the forward model. The adjustment consists in applying a multiplicative factor to the water vapor profile from the CTH to the Top of Atmosphere (TOA), noted $WVPAC$, at each iteration. The resulting adjustment coefficient is derived by calculating the ratio between the estimated $IWVAC$ at iteration $i+1$ and the one estimated at iteration i:

$$WVPAC_{i+1}(z) = \beta \cdot WVPAC_i(z) \tag{5}$$

with,

$$\beta = \frac{IWVAC_{i+1}}{IWVAC_i} \tag{6}$$

the adjustment coefficient.

4 Sensitivity of water vapor spectral bands to IWV AC

In this section, we examine how the radiances simulated in the water vapor spectral bands (1.13 and 1.37 µm) varying with $IWVAC$ (figure 3). Simulations have been performed with atmospheric profiles derived from the Air Force Geophysics Laboratory (AFGL) database (Anderson et al., 1986).

By decreasing the CTH in our cloud simulation input, we increase the $IWVAC$. Figure 3 shows our radiative transfer simulations results: a decrease in the simulated radiance is observed as $IWVAC$ increases. Indeed, the greater the apparent

https://doi.org/10.5194/egusphere-2024-1560
Preprint. Discussion started: 4 June 2024

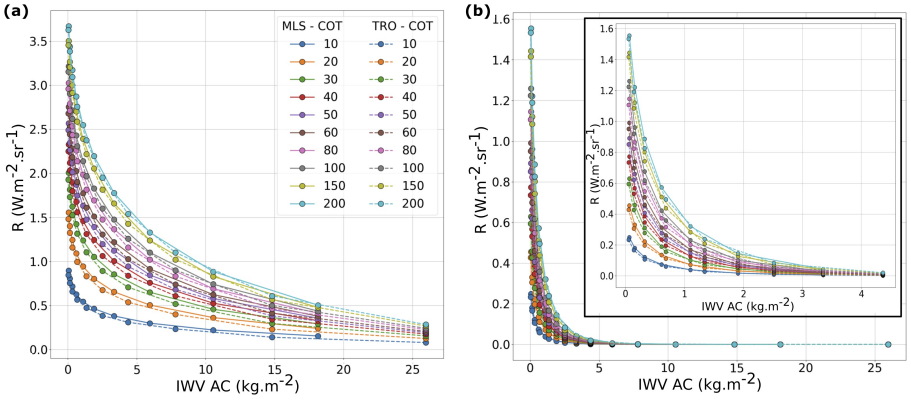

Figure 3. Simulated radiances of the C^{3}IEL 1.13 µm band (a) and the 1.37 µm band (b) as a function of $IWVAC$ for two atmospheric profiles from the AFGL database (Mid-Latitude Summer and Tropical profiles), for several Cloud Top Heights (CTH = 1, 2, 3, 4, 5, 6, 7, 8, 9, and 10 km), and various COT ranging from 10 to 200. In the figure (b), the rectangle represents a zoom of the figure for $IWVAC$ values between approximately 0 and 5 $\mathrm{kg.m^{-2}}$.

path of radiation through the atmosphere is, the higher is the amount of water vapor with which the radiation interacts. Consequently, water vapor absorption increases, resulting to a decrease in radiances. Radiance sensitivity is particularly high for lower water vapor contents but decreases as water vapor content increases.

Radiance for the 1.37 µm spectral band becomes negligible when water vapor content exceeds 5 $\mathrm{kg.m^{-2}}$, while it does not reach zero in the 1.13 µm band for values until 30 $\mathrm{kg.m^{-2}}$. The 1.37 µm band will mainly be useful in retrieving $IWVAC$ either in the presence of high-level clouds or in a dry atmosphere. It is also worth noting the non-overlapping color curves (each color corresponds to a value of COT). Despite the slight difference between them, this indicates a slight sensitivity of these two spectral bands to COT.

5 IWV AC retrieval

The retrieval algorithm presented in this paper was firstly tested under idealized cloudy sky conditions using clear sky profiles from the AFGL database (Anderson et al., 1986), and then under realistic cloudy sky conditions, using atmospheric profiles provided by ECMWF-IFS database (https://www.nwpsaf.eu/site/software/atmospheric-profile-data/) to better evaluate its performance.

5.1 Under idealized cloudy sky conditions

In the AFGL database profiles, we have artificially introduced a cloud with base (CBH) fixed at 0.2 km and with 10 Cloud Top Height values (CTH = 1, 2, 3, 4, 5, 6, 7, 8, 9, and 10 km). The COT varies from 10 to 200. The solar incidence angle

https://doi.org/10.5194/egusphere-2024-1560
Preprint. Discussion started: 4 June 2024

is set to 30 ° and the satellite observation angle is 0 ° (nadir). The target *IWV AC* values are derived from the AFGL tropical profile, while the first guess profile used to start the retrieval process is the SAS (Sub-Arctic Summer) profile.

As the relation between non-absorbing radiances and COT is well-known and widely used, figures related to the COT retrieval are not displayed here. Nevertheless, the developed retrieval algorithm allows to retrieve COT with an error less than 10 % for COT values below 100 (less than 5 % for values below 50). However, as it is well-known (*e.g.,* Nakajima and King, 1990; Nakajima et al., 1991), if the COT exceed 100, the retrieval is more uncertain because of the asymptotic behavior of the radiances as a function of cloud optical thickness for large COT values.

The $IWVAC$ retrieval is tested for two measurement vectors: one with only the 1.13 µm radiances and the others with the two water vapor channels centered at 1.13 and 1.37 µm. Absolute errors are displayed in figure 4. The retrievals were realized with CTH range and water vapor profiles corresponding to $IWVAC$ values within the approximate range of 10^{-2} kg.m^{-2} to 26 kg.m^{-2}.

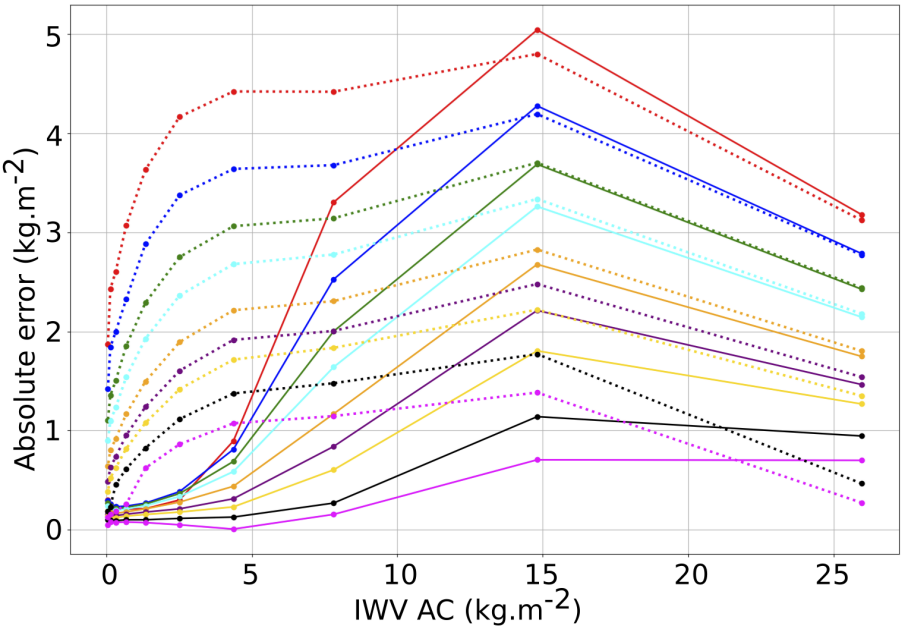

Figure 4. Absolute errors obtained for the $IWVAC$ retrieval ($IWVAC$ retrieved - $IWVAC$ target) as a function of the $IWVAC$ target values. Dotted lines represent results obtained using only the 1.13 µm spectral band, while full lines illustrate results when using both spectral bands (1.13 and 1.37 µm) in the measurement vectors. Each color corresponds to a specific COT value: 10 (red), 20 (blue), 30 (green), 40 (cyan), 60 (orange), 80 (purple), 100 (yellow), 150 (black) and 200 (magenta).

Whatever the measurement vector used (one or two radiances), an increase in the absolute error of the retrieved $IWVAC$ is observed when the water vapor content increases, as well as when the COT decreases. In other words, optically thin clouds exhibit a more pronounced absolute error because of a greater vertical penetration into the cloud. The radiation apparent path through the atmosphere is longer in such cases, which leads to increase the absorption difference in the cloud. As illustrated

https://doi.org/10.5194/egusphere-2024-1560
Preprint. Discussion started: 4 June 2024

by Albert et al. (2001), the simultaneous influences of enhanced vertical penetration into the cloud and multiple scattering contribute to increased water vapor absorption, thereby disrupting the retrieval process and decreasing the accuracy of the $IWVAC$ retrieval. We also observe that the absolute error (retrieved minus target values) is always positive, which means that the retrieved $IWVAC$ is consistently overestimated. For each case, the assumed extinction profile used to generate the dataset of idealized radiances and that defined in the model are similar, the difference comes from the water vapor profile within the cloud. Indeed, in the retrieval process, the profile within the cloud is not adjusted. The first guess profile (AFGL SAS profile) is drier than the target AFGL tropical profile. Consequently, less radiation is absorbed in the cloud, and to compensate it, the retrieved water vapor content above the cloud is greater.

When considering only the simulated radiance at 1.13 µm (dotted lines on figure 4), absolute errors increases rapidly for $IWVAC$ values below 5 kg.m^{-2}. Subsequently, they tend to stabilize between 1 and 2 kg.m^{-2} for higher optical thicknesses, and approximately 5 kg.m^{-2} for lower optical thicknesses (*e.g.*,, $COT = 10$, red curve).

When we examine the combined information from both spectral bands (solid lines), the absolute error significantly decreases to values below 1 kg.m^{-2} for water vapor contents below 5 kg.m^{-2}, regardless of the optical thickness values. In cases where the water vapor content is higher, particularly when $COT > 100$ (black and magenta curves), the absolute error in the retrieved $IWVAC$ remains below 1 kg.m^{-2}. For water vapor contents exceeding 15 kg.m^{-2}, the contribution of the 1.37 kg.m^{-2} spectral band becomes negligible, except for very high optical thicknesses. Comparing retrievals conducted only with the 1.13 µm spectral band and those integrating radiances from both spectral bands, as excepted, the benefit of the 1.37 µm band is notable, especially for low water vapor contents corresponding to situations with high CTH. Utilizing both spectral bands enables the achievement of absolute errors close to 0.2 to 0.3 kg.m^{-2} for $IWVAC$ values below approximately 1.5 kg.m^{-2}.

5.2 Under realistic cloudy sky conditions

The ECMWF-IFS database provides realistic atmospheric cloud profiles at 137 pressure levels, encompassing profiles of temperature, specific humidity, Cloud Liquid Water (CLW), and Cloud Ice Water (CIW), in addition to the cloud coverage. It also incorporates surface data (pressure, temperature, albedo) and details regarding latitude, longitude, and date.

5.2.1 Realistic water vapor profiles

We only use profiles containing clouds located above the ocean, as the developed algorithm is currently not taking into account the surface below clouds. Profiles at latitudes higher than 60 ° N/S are also excluded, as the C^{3}IEL mission will not make observations at such latitudes. Furthermore, the C^{3}IEL mission focuses on studying *cumulus congestus* and *cumulonimbus* clouds. Consequently, clear sky profiles and those containing only cirrus clouds have been discarded from our study. Figure 5 shows the geographical distribution of the selected profiles. For each profile, we have calculated the $IWVAC$, which is the target value used as the "truth". The distribution of these values are presented in figure 6.

For low/mid-level clouds, $IWVAC$ values range from 0.6 to 30 kg.m^{-2} but are predominantly below 15 kg.m^{-2}. For high-level clouds, the values range from approximately 10^{-3} kg.m^{-2} to 4 kg.m^{-2} (mostly below 1.5 kg.m^{-2}). Initially, the

https://doi.org/10.5194/egusphere-2024-1560
Preprint. Discussion started: 4 June 2024

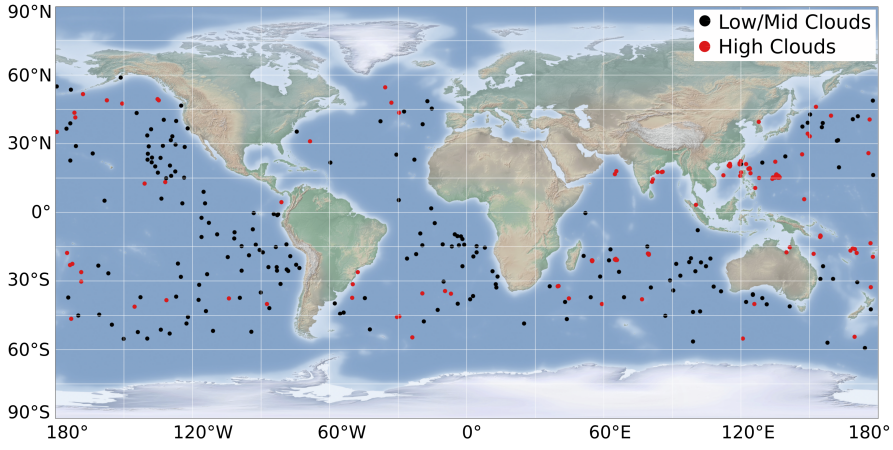

Figure 5. Geographical distribution of the selected profiles from the ECMWF-IFS database used to test the developed retrieval algorithm. A total of 338 profiles, including 196 profiles with low/mid-level clouds, only liquid (black points), and 142 profiles with high-level/mixed-phase clouds (red points) are selected.

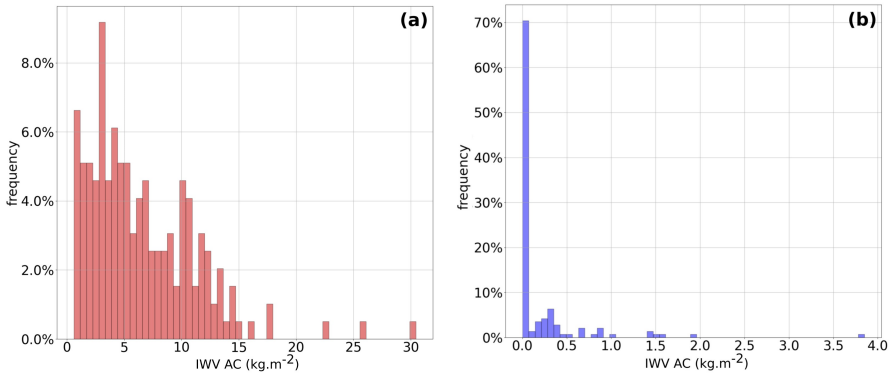

Figure 6. Distribution of $IWVAC$ values calculated from the selected profiles. (a) target $IWVAC$ values for the 196 profiles containing low/mid-level clouds, (b) target values for the 142 profiles containing high-level clouds.

database did not include enough clouds at mid-high top altitudes. To compensate for this deficiency, the CTH were artificially decreased by 4 km. Consequently, the $IWVAC$ calculations for high-level clouds were derived from these adjusted profiles.

5.2.2 Results of the IWV AC retrieval: Low/Mid-level clouds

The simulations are made using the Solar Zenith Angle (SZA) and the Solar Azimuth Angle (SAA) computed based on information regarding latitude, longitude, date, and time linked to the diverse profiles. As for retrievals under idealized conditions, we have focused on the $IWVAC$ retrieval. However, as mentioned earlier, the developed algorithm also enables the

https://doi.org/10.5194/egusphere-2024-1560
Preprint. Discussion started: 4 June 2024

1D equivalent COT retrieval. Under realistic conditions and if $COT < 100$, the algorithm has shown a good ability to retrieve the COT with a bias of 0.02 (0.2 % relative error) and a RMSE of 0.06, on the retrieved values. However, if $COT > 100$, the COT retrieval exhibits large errors due to the asymptotic variations of the radiance as a function of COT. Figure 7 illustrates the relationship between the retrieved values and the target values for the 196 profiles containing a low/mid-level cloud.

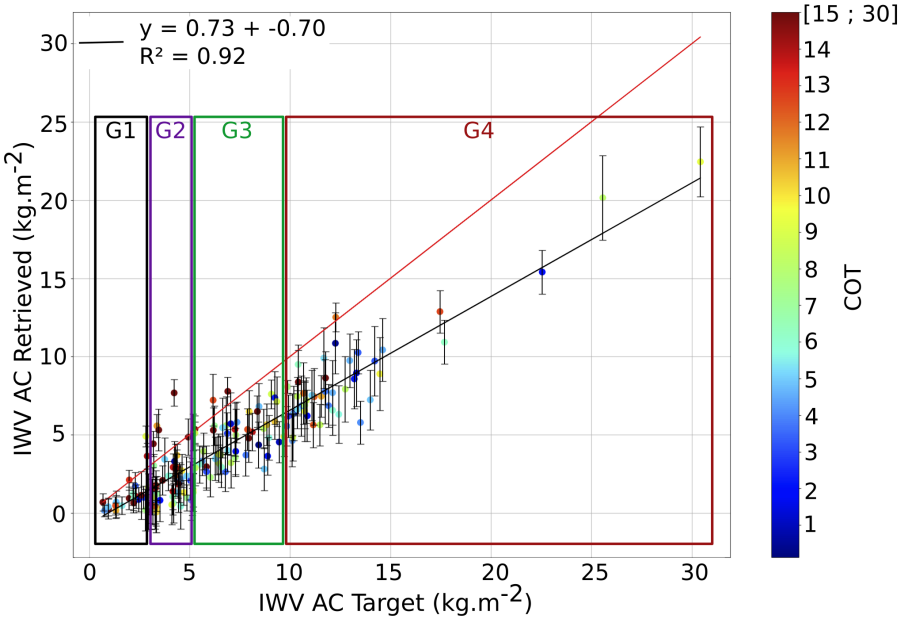

Figure 7. Relationship between the retrieved and target $IWVAC$ values for profiles containing a low/mid-level cloud. The color code represents the COT, the black line is the linear regression line between these two variables, and the red line is the line $y = x$. The black error bars represent the uncertainty estimated by the retrieval algorithm.

A strong correlation is observed between the retrieved and target values, as indicated by a score (R^2) of 0.92. A convergence rate of 87 % is also calculated. The linear regression between the two variables is shifted from the $y = x$ line, with a slope less than 1. This suggests that, in the majority of cases (94 %), the retrieved $IWVAC$ is underestimated. The reasons of this underestimation will be detailed in section 5.2.4. A bias of 2.63 $\mathrm{kg.m^{-2}}$ and a RMSE of 3.23 $\mathrm{kg.m^{-2}}$ is obtained. To refine and better characterize the bias and the RMSE across various ranges of $IWVAC$ values, we have classified the values according to the "true" $IWVAC$. Four groups have been defined, illustrated by distinct rectangles in figure 7. For each group, both the bias and RMSE have been calculated (table 2).

Logically, the bias and RMSE increase as the $IWVAC$ increases. This increase is related to the larger value of the $IWVAC$ and to the decrease of the sensitivity of the C^{3}IEL water vapor spectral bands (1.13 and 1.37 µm) when $IWVAC$ increases (figure 3).

The error bars represent the *a posteriori* random uncertainty estimated by the retrieval algorithm. These errors comes from the errors measurement and the fixed (or non-retrieved parameters). However, as already seen in section 5.1 with the idealized

https://doi.org/10.5194/egusphere-2024-1560
Preprint. Discussion started: 4 June 2024

Table 2. Bias and RMSE calculated for the four classes of target $IWVAC$ values, as illustrated by the rectangles in figure 7. G1: < 3 $\mathrm{kg.m^{-2}}$, G2: [3 ; 6[$\mathrm{kg.m^{-2}}$, G3: [6 ; 9[$\mathrm{kg.m^{-2}}$, and G4: > 9 $\mathrm{kg.m^{-2}}$.

$IWVAC$	G1	G2	G3	G4
bias	0.99 $\mathrm{kg.m^{-2}}$	1.99 $\mathrm{kg.m^{-2}}$	2.63 $\mathrm{kg.m^{-2}}$	4.13 $\mathrm{kg.m^{-2}}$
RMSE	1.42 $\mathrm{kg.m^{-2}}$	2.55 $\mathrm{kg.m^{-2}}$	3.01 $\mathrm{kg.m^{-2}}$	4.46 $\mathrm{kg.m^{-2}}$

profiles, it exists a bias related to the assumption made in the forward model for the extinction (homogeneous plane-parallel approximation) and water vapor profiles. Consequently, the retrieved value is underestimated and the *a posteriori* error capture the target only in 16 % of the cases. It highlights the limitation of the developed algorithm to accurately take into account the non-Gaussian errors, *e.g.* coming from the radiative transfer assumptions. Indeed, since no information is available regarding these profiles in the measurements, the typical assumption of vertical uniformity is employed and, errors related to it are not included in the error variance-covariance matrix, which contains only the random part of the Gaussian error distribution. In the future, ways of improvement can be to look for and use a representative model with a non-uniform extinction profile to reduce the bias or to compute the error due to the forward model as done in Matar et al. (2023).

5.2.3 Results of the IWV AC retrieval: High-level clouds

Results for clouds with a significant vertical development and a high CTH (142 cloud profiles) are presented in figure 8. For this type of clouds, the COT values exceeds 100, while $IWVAC$ values are generally low, below 1.5 $\mathrm{kg.m^{-2}}$ (figure 6 (b)). In terms of COT retrieval, the errors become considerable for such high values as beyond an optical thickness of 100, the spectral band sensitivity at 1.04 µm is not sufficient for a reliable retrieval, under the assumption of an infinite cloud. However, as measured radiances are saturated for such values, it should not impact the $IWVAC$ retrieval.

In comparison with figure 7, the convergence rate in this context is significantly reduced, with a rate of 14 % for high-level clouds. For very low $IWVAC$ values enclosed within the black rectangle (< 0.2 $\mathrm{kg.m^{-2}}$), the sensitivity of the measurements including an uncertainty of 5 % is clearly not sufficient for a consistent retrieval. The retrievable threshold of the current retrieval algorithm is currently hard to estimate but certainly over 0.2 $\mathrm{kg.m^{-2}}$ and have to be confirmed with more cases in the future.

5.2.4 Discussion concerning the underestimation of the retrieved IWV AC

As stated in the figure 7 comments, there is a notable underestimation rate of the retrieved value (94 %). We have identified two scenarios that could explain the underestimation of the water vapor content above the cloud presented in figure 9. The figures show two examples of realistic absolute humidity and extinction profiles within the cloud coming from the ECMWF-IFS database (green and red solid lines respectively) and those retrieved and used in the cloud model designed for the retrieval algorithm (purple solid line and dashed red lines respectively).

https://doi.org/10.5194/egusphere-2024-1560
Preprint. Discussion started: 4 June 2024

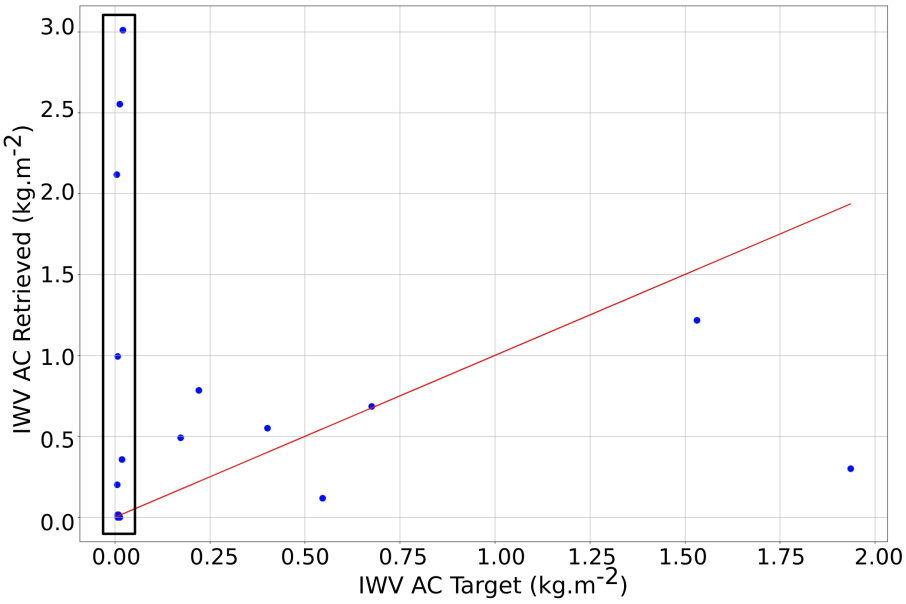

Figure 8. Relationship between the retrieved $IWVAC$ value and the target value for profiles containing a high-level cloud. The red line represents the line $y = x$.

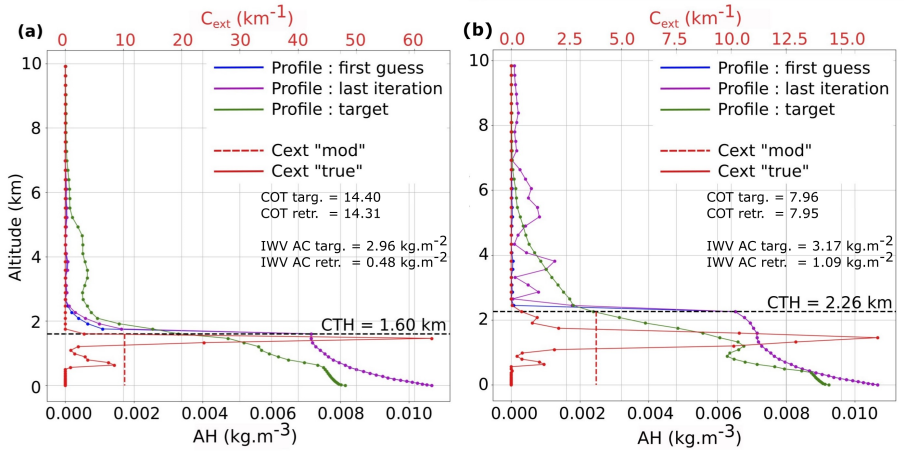

Figure 9. Absolute humidity and extinction profiles within the cloud: realistic profiles derived from the ECMWF-IFS database and retrieved (above the cloud) and assumed profiles in the cloud model used for the developed retrieval algorithm. Two cases are showed to explain the underestimation of $IWVAC$. The dashed black line indicates the CTH. The green curve illustrates the "true" water vapor profile, the blue curve represents the "first guess" water vapor profile, and the purple curve defines the profile adjusted in the latest iteration. The solid red curve depicts the "true" cloud extinction profile, while the dashed red line represents the cloud model extinction profile.

https://doi.org/10.5194/egusphere-2024-1560
Preprint. Discussion started: 4 June 2024

In figure 9 (a), in the upper layers of the cloud, the model extinction profile in the cloud is characterized by a lower value compared to the "true" extinction profile. This implies a greater vertical penetration of the radiation into the cloud comparing to what occurs in the realistic profile, thus a greater absorption by water vapor. Additionally, the water vapor profile defined in the model, corresponding to 100 % humidity, exceeds the "true" water vapor profile. Consequently, the absorption by water vapor is greater for the cloud model than in the realistic cloud. Both effect lead to a lower retrieved $IWVAC$ value comparing to the target value, because the retrieval algorithm tends to compensate the higher absorption in the cloud model inversion with a lower absorption above the cloud in order to minimize the difference between the measured (y in Eq. (1)) and simulated radiances $F(x, b)$.

In figure 9 (b), in the upper part of the cloud, the extinction profile of the cloud model inversion exceeds the "true" extinction profile. The vertical penetration into the cloud is thus reduced in the inversion compared to reality, which should lead to an overestimation of the $IWVAC$. However, the model water vapor profile shows a higher content in the upper part of the cloud compared to the "true" water vapor profile. As a result, although the vertical penetration into the cloud is lower in the model, the radiation encounter a greater amount of water vapor than in the realistic cloud. This effect predominates, which tends to show that the water vapor profile used here as first guess is probably too much humid in the upper layers of the cloud.

5.2.5 Consideration concerning the use the combination of both the 1.13 and 1.37 µm water vapor spectral bands

In Section 5.1, we have illustrated how the combination of the two water vapor spectral bands from the C^{3}IEL mission leads to a significant reduction in the absolute error under idealized conditions (figure 4). This section aims to check the interest of combining the two water vapor bands on the $IWVAC$ retrieval from realistic profiles. Table 3 presents the convergence rate, the bias and RMSE for retrievals using both combined water vapor spectral bands and using only the 1.13 µm spectral band.

Table 3. Convergence rate, bias and RMSE on the $IWVAC$ retrieval for realistic cloud profiles (low/mid-level cloud) by combining both water vapor spectral bands and using only the 1.13 µm band.

	convergence rate	bias	RMSE
[1.13 + 1.37] µm	87 %	2.63 kg.m^{-2}	3.23 kg.m^{-2}
1.13 µm	69 %	2.94 kg.m^{-2}	4.29 kg.m^{-2}

The combination of the two channels improves the convergence rate from 69 % to 87 %. In addition, combining the two spectral bands leads to a 11 % decrease in bias and a 25 % reduction in RMSE.

6 Conclusions

The objective of this study is to develop a retrieval algorithm in order to estimate the Integrated Water Vapor content Above Cloud ($IWVAC$), in the context of a future space mission project named C^{3}IEL (Cluster for Cloud evolution, ClImatE, and Lightning). This mission aims at investigating the development of convective clouds with a high spatial and temporal resolu-

https://doi.org/10.5194/egusphere-2024-1560
Preprint. Discussion started: 4 June 2024

tion, the electrical activity associated with these clouds, and the water vapor content above and around cloud. The developed algorithm is based on a Bayesian probabilistic approach, the Optimal Estimation Method (OEM), which is an iterative least square fitting method that permits to consider a certain number of parameters (fixed parameters, *a priori* knowledge, *etc.*) as well as associated uncertainties for the estimation of several variables.

A study has been conducted to assess the sensitivity of the three SWIR spectral bands of the C^{3}IEL mission to the Cloud Optical Thickness (COT) and the Integrated Water Vapor content Above Cloud ($IWVAC$). In this paper, we mainly focus on the $IWVAC$ parameters as the retrieval of COT from non-absorbing band is already well documented in numerous publications. Using simulations in the two water vapor spectral bands (1.13 and 1.37 µm), we shows that radiance value decreases as $IWVAC$ increases and thus water vapor absorption. We note that the simulated radiances in the highly absorbing band (1.37 µm) tends toward 0 for $IWVAC$ values greater than 5 kg.m^{-2}, *i.e.,* emphasizing the fact that this band will be useful for low $IWVAC$, in dry atmosphere or above high clouds.

The developed algorithm is first tested under idealized cloudy sky conditions with homogeneous profiles as assumed in the inversion model used for the algorithm. We confirm the existence of an upper limit for COT retrieval, which is around 100. Concerning the $IWVAC$ retrieval from the absorption bands, the absolute error tends to increase as $IWVAC$ increases and the COT decreases. This suggests that the absolute error in $IWVAC$ becomes more significant for optically thin clouds due to penetration in the cloud and multiple scattering. We have also illustrated the advantages of combining the two water vapor spectral bands, specifically, for the low water vapor content values where the absolute error when combining the two spectral bands stays below 0.5 kg.m^{-2}, regardless of cloud optical thickness.

Then, we tested the algorithm on realistic profiles obtained from the ECMWF-IFS database. Our focus was on profiles featuring exclusively cloudy sky conditions over the ocean and within a latitude range of 60 ° N/S. We have identified 196 cloudy profiles containing low/mid-level clouds and 142 profiles containing high-level clouds (excluding cirrus). The algorithm exhibited a 87 % convergence rate for realistic profiles with low/mid-level clouds. Regarding the $IWVAC$, there is a strong correlation between the retrieved values and the target values (R^2 of 0.92). The overall bias in the retrieval amounts to 2.63 kg.m^{-2}, with a quasi-systematic underestimation of the retrieved $IWVAC$. We have showed that this underestimation results from a combined effect of the vertical penetration into the cloud related to the extinction and water vapor profiles. Finally, we showed that the combination of the two bands effectively reduces bias and RMSE. For low $IWVAC$ in the presence of high-level clouds, the iteration process fails most of the time. A minimum threshold of at least 0.2 kg.m^{-2} seems required for a consistent $IWVAC$ retrieval.

The algorithm presented in this paper is a preliminary one, short-term improvements remain necessary. An improvement that appears to be required to refine uncertainty estimation and potentially the retrieved $IWVAC$ value is to use a more realistic extinction profile in the cloud inversion model. However, at our knowledge no simple analytic profile for convective clouds exists. Analysis of profiles from radar observations or from cloud simulation as in Shang et al. (2023) has thus te be realized in a first step. Currently, the algorithm works only for profiles with clouds over the ocean. Thus, as the C^{3}IEL mission will also observe convective clouds over land, the algorithm need to be extended for these cases. In addition, research works has to be done to exploit the multi-views of the C^{3}IEL mission that could reduce the bias by better constraining the retrieval.

https://doi.org/10.5194/egusphere-2024-1560
Preprint. Discussion started: 4 June 2024

Appendix A: Variables from the *a posteriori* variance-covariance matrix

In our study, the *a priori* variance-covariance matrix (see Eq. (4)) is a diagonal matrix where the diagonal terms are the squared standard deviations for each parameter contained in the *a priori* state vector:

$$S_a = \begin{bmatrix} \sigma^2_{COT} & 0 \\ 0 & \sigma^2_{IWVAC} \end{bmatrix} \tag{A1}$$

with σ_{COT} and σ_{IWVAC} obtained by multiplying the *a priori* state vector x_a by the arbitrarily chosen *a priori* error.

S_ϵ, the error variance-covariance matrix is expressed, in our study, as follows:

$$S_\epsilon = S_y + S_{fp} \tag{A2}$$

S_y is the measurement variance-covariance matrix, and S_{fp} describes the variance-covariance matrix linked to the fixed parameters:

$$S_y = \begin{bmatrix} \sigma^2_{y1} & 0 & 0 \\ 0 & \sigma^2_{y2} & 0 \\ 0 & 0 & \sigma^2_{y3} \end{bmatrix} \tag{A3}$$

and,

$$S_{fp} = K_b S_b K_b^T \tag{A4}$$

with,

$$K_b = \left.\frac{dF(b)}{db}\right|_x = \left.\frac{F(b+db) - F(b)}{db}\right|_x \tag{A5}$$

where b represent the fixed parameter (see table 1) and db is equal to 1 % of the fixed parameter value. S_b is a diagonal matrix whose diagonal elements represent the squared standard deviation associated with the different fixed parameters of the forward model:

$$S_b = \begin{bmatrix} \sigma^2_{Albedo} & 0 & 0 & 0 & 0 \\ 0 & \sigma^2_{CBH} & 0 & 0 & 0 \\ 0 & 0 & \sigma^2_{CTH} & 0 & 0 \\ 0 & 0 & 0 & \sigma^2_{Reff,droplet} & 0 \\ 0 & 0 & 0 & 0 & \sigma^2_{Reff,ice} \end{bmatrix} \tag{A6}$$

The different elements of this matrix are obtained by calculating the product of the relevant fixed parameter with the uncertainty attributed to it (see table 1).

Author contributions. Each author has played a significant role in the development and scientific exploration presented in this study. RP performed the study and write the original draft of the article. CC provided support for radiative transfer simulations and the analysis

https://doi.org/10.5194/egusphere-2024-1560
Preprint. Discussion started: 4 June 2024

of corresponding data and retrieval results. OP and GP contributed to the analysis of the atmospheric database (ECMWF-IFS) and the interpretation of retrieval results as well. CP offered expertise in the optimal estimation method and contributed to the analysis of radiative transfer simulations and retrieval outcomes. FT contributed to the development of the retrieval algorithm.

Competing interests. There is no competing interests.

Acknowledgements. We are grateful to the CNES/TOSCA program which has funded this work as part of the preparation of the Cluster for Cloud evolution, Climate and Lightning French-Israeli space mission project. We acknowledge the AERIS/ICARE data center for providing the ARTDECO radiative transfer code free of charge. We would also like to thank L-C. Labonnote for his precious help and expertise on the ARTDECO tool.

https://doi.org/10.5194/egusphere-2024-1560
Preprint. Discussion started: 4 June 2024

References

Albert, P., Bennartz, R., and Fischer, J.: Remote Sensing of Atmospheric Water Vapor from Backscattered Sunlight in Cloudy Atmospheres, Journal of Atmospheric and Oceanic Technology, https://doi.org/10.1175/1520-0426(2001)018<0865:RSOAWV>2.0.CO;2, 2001.

Anderson, G. P., Chetwynd, J. H., and She, E. P.: AFGL Atmospheric Constituent Profiles (0-120km), p. 47, 1986.

Bennartz, R. and Fischer, J.: Retrieval of columnar water vapour over land from backscattered solar radiation using the Medium Resolution Imaging Spectrometer, Remote Sensing of Environment, pp. 274–283, https://doi.org/10.1016/S0034-4257(01)00218-8, 2001.

Blyth, A. M.: Entrainment in Cumulus Clouds, American Meteorological Society, https://doi.org/10.1175/1520-0450(1993)032<0626:eicc>2.0.co;2, 1993.

Bony, S., Stevens, B., Frierson, D. M. W., Jakob, C., Kageyama, M., Pincus, R., Shepherd, T. G., Sherwood, S. C., Siebesma, A. P., Sobel, A. H., Watanabe, M., and Webb, M. J.: Clouds, circulation and climate sensitivity, Nature Geoscience, pp. 261–268, 2015.

Bouffiès, S., Bréon, F. M., Tanré, D., and Dubuisson, P.: Atmospheric water vapor estimate by a differential absorption technique with the polarisation and directionality of the Earth reflectances (POLDER) instrument, Journal of Geophysical Research: Atmospheres, pp. 3831–3841, https://doi.org/10.1029/96JD03126, 1997.

Crutzen, P. J. and Ramanathan, V.: The Parasol Effect on Climate, Science, pp. 1679–1681, https://doi.org/10.1126/science.302.5651.1679, 2003.

Dandini, P., Cornet, C., Binet, R., Fenouil, L., Holodovsky, V., Y. Schechner, Y., Ricard, D., and Rosenfeld, D.: 3D cloud envelope and cloud development velocity from simulated CLOUD (C3IEL) stereo images, Atmospheric Measurement Techniques, pp. 6221–6242, https://doi.org/10.5194/amt-15-6221-2022, 2022.

de Haan, J. F., Bosma, P. B., and Hovenier, J. W.: The adding method for multiple scattering calculations of polarized light, Astronomy and Astrophysics, 1987.

Desbois, M., Capderou, M., Eymard, L., Roca, R., Viltard, N., Viollier, M., and Karouche, N.: Megha-Tropiques : un satellite hydrométéorologique franco-indien, La Météorologie, https://doi.org/10.4267/2042/18185, 2007.

Dubuisson, P., C.-Labonnote, L., Riedi, J., Compiègne, M., and Winiarek, V.: ARTDECO : Atmospheric Radiative Transfer Database for Earth and Climate Observation, in: International Radiation Symposium, Auckland, New Zealand, 2016.

Fermepin, S. and Bony, S.: Influence of low-cloud radiative effects on tropical circulation and precipitation, Journal of Advances in Modeling Earth Systems, pp. 513–526, https://doi.org/10.1002/2013MS000288, 2014.

Gao, B. C. and Kaufman, Y. J.: Water vapor retrievals using Moderate Resolution Imaging Spectroradiometer (MODIS) near-infrared channels, Journal of Geophysical Research: Atmospheres, https://doi.org/10.1029/2002jd003023, 2003.

Harrison, E. F., Minnis, P., Barkstrom, B. R., Ramanathan, V., Cess, R. D., and Gibson, G. G.: Seasonal variation of cloud radiative forcing derived from the Earth Radiation Budget Experiment, Journal of Geophysical Research: Atmospheres, https://doi.org/10.1029/JD095iD11p18687, 1990.

Hilton, F., Armante, R., August, T., Barnet, C., Bouchard, A., Camy-Peyret, C., Capelle, V., Lieven, C., Clerbaux, C., Coheur, P.-F., Collard, A., Crevoisier, C., Dufour, G., Edwards, D., Faijan, F., Fourrié, N., Gambacorta, A., Goldberg, M., Guidard, V., Hurtmans, D., Illingworth, S., Jacquinet-Husson, N., Kerzenmacher, T., Klaes, D., Lavanant, L., Masiello, G., Matricardi, M., McNally, A., Newman, S., Pavelin, E., Payan, S., Péquignot, E., Peyridieu, S., Phulpin, T., Remedios, J., Schlüssel, P., Serio, C., Strow, L., Stubenrauch, C., Taylor, J., Tobin, D., Wolf, W., and Zhou, D.: Hyperspectral Earth Observation from IASI: Five Years of Accomplishments, Bulletin of the American Meteorological Society, https://doi.org/10.1175/BAMS-D-11-00027.1, 2012.

https://doi.org/10.5194/egusphere-2024-1560
Preprint. Discussion started: 4 June 2024

Jensen, E. J., Toon, O. B., Selkirk, H. B., Spinhirne, J. D., and Schoeberl, M. R.: On the formation and persistence of subvisible cirrus clouds near the tropical tropopause, Journal of Geophysical Research: Atmospheres, https://doi.org/10.1029/95JD03575, 1996.

Karbou, F., Aires, F., Prigent, C., and Eymard, L.: Potential of Advanced Microwave Sounding Unit-A (AMSU-A) and AMSU-B measurements for atmospheric temperature and humidity profiling over land, Journal of Geophysical Research: Atmospheres, https://doi.org/10.1029/2004JD005318, 2005.

King, M. D., Platnick, S., Yang, P., Arnold, G. T., Gray, M. A., Riedi, J. C., Ackerman, S. A., and Liou, K.-N.: Remote Sensing of Liquid Water and Ice Cloud Optical Thickness and Effective Radius in the Arctic: Application of Airborne Multispectral MAS Data, Journal of Atmospheric and Oceanic Technology, pp. 857–875, https://doi.org/10.1175/1520-0426(2004)021<0857:RSOLWA>2.0.CO;2, 2004.

Lee, J., Yang, P., Dessler, A. E., Gao, B.-C., and Platnick, S.: Distribution and Radiative Forcing of Tropical Thin Cirrus Clouds, Journal of the Atmospheric Sciences, https://doi.org/10.1175/2009JAS3183.1, 2009.

Leonarski, L., C.-Labonnote, L., Compiègne, M., Vidot, J., Baran, A. J., and Dubuisson, P.: Potential of Hyperspectral Thermal Infrared Spaceborne Measurements to Retrieve Ice Cloud Physical Properties: Case Study of IASI and IASI-NG, Remote Sensing, https://doi.org/10.3390/rs13010116, 2020.

Masson-Delmotte, V. P., Zhai, A., Pirani, S. L., Connors, C., Péan, S., Berger, N., Caud, Y., Chen, L., Goldfarb, M. I., Gomis, M., Huang, K., Leitzell, E., Lonnoy, J. B. R., Matthews, T. K., Maycock, T., Waterfield, O., Yelekçi, R. Y., and Zhou, B.: Climate Change 2021: The Physical Science Basis. Contribution of Working Group I to the Sixth Assessment Report of the Intergovernmental Panel on Climate Change, Cambridge University Press. In Press., 2021.

Matar, C., Cornet, C., Parol, F., C.-Labonnote, L., Auriol, F., and Nicolas, M.: Liquid cloud optical property retrieval and associated uncertainties using multi-angular and bispectral measurements of the airborne radiometer OSIRIS, Atmospheric Measurement Techniques, https://doi.org/10.5194/amt-16-3221-2023, 2023.

McFarquhar, G. M., Heymsfield, A. J., Spinhirne, J., and Hart, B.: Thin and Subvisual Tropopause Tropical Cirrus: Observations and Radiative Impacts, Journal of the Atmospheric Sciences, https://doi.org/10.1175/1520-0469(2000)057<1841:TASTTC>2.0.CO;2, 2000.

Nakajima, T. and King, M. D.: Determination of the Optical Thickness and Effective Particle Radius of Clouds from Reflected Solar Radiation Measurements. Part I: Theory, Journal of the Atmospheric Sciences, pp. 1878–1893, https://doi.org/10.1175/1520-0469(1990)047<1878:DOTOTA>2.0.CO;2, 1990.

Nakajima, T., King, M. D., Spinhirne, J. D., and Radke, L. F.: Determination of the Optical Thickness and Effective Particle Radius of Clouds from Reflected Solar Radiation Measurements. Part II: Marine Stratocumulus Observations, Journal of Atmospheric Sciences, pp. 728–751, https://doi.org/10.1175/1520-0469(1991)048<0728:DOTOTA>2.0.CO;2, 1991.

Ramanathan, V., Cess, R. D., Harrison, E. F., Minnis, P., Barkstrom, B. R., Ahmad, E., and Hartmann, D.: Cloud-Radiative Forcing and Climate: Results from the Earth Radiation Budget Experiment, Science, pp. 57–63, https://doi.org/10.1126/science.243.4887.57, 1989.

Rao, T. N., Sunilkumar, K., and Jayaraman, A.: Validation of humidity profiles obtained from SAPHIR, on-board Megha-Tropiques, CURRENT SCIENCE, 2013.

Rodgers, C. D.: Inverse Methods for Atmospheric Sounding: Theory and Practice, Series on Atmospheric, Oceanic and Planetary Physics, WORLD SCIENTIFIC, ISBN 978-981-02-2740-1 978-981-281-371-8, https://doi.org/10.1142/3171, 2000.

Rosenfeld, D., Cornet, C., Aviad, S., Binet, R., Crebassol, P., Dandini, P., Defer, E., Deschamps, A., Fenouil, L., Frid, A., Holodovsky, V., Kaidar, A., Peroni, R., Pierangelo, C., Price, C., Ricard, D., Schechner, Y., and Yair, Y.: C3IEL: Cluster for Cloud Evolution, ClImatE and Lightning, 2022.

https://doi.org/10.5194/egusphere-2024-1560
Preprint. Discussion started: 4 June 2024

Rosenkranz, P. W.: Retrieval of temperature and moisture profiles from AMSU-A and AMSU-B measurements, IEEE Transactions on Geoscience and Remote Sensing, https://doi.org/10.1109/36.964979, 2001.

Schlüssel, P. and Goldberg, M.: Retrieval of atmospheric temperature and water vapour from IASI measurements in partly cloudy situations, Advances in Space Research, https://doi.org/10.1016/S0273-1177(02)00101-1, 2002.

Schmidt, G. A., Ruedy, R. A., Miller, R. L., and Lacis, A. A.: Attribution of the present-day total greenhouse effect, Journal of Geophysical Research, https://doi.org/10.1029/2010JD014287, 2010.

Schneider, T., O'Gorman, P. A., and Levine, X. J.: WATER VAPOR AND THE DYNAMICS OF CLIMATE CHANGES, Reviews of Geophysics, https://doi.org/10.1029/2009RG000302, 2010.

Shang, H., Hioki, S., Penide, G., Cornet, C., Letu, H., and Riedi, J.: Establishment of an analytical model for remote sensing of typical stratocumulus cloud profiles under various precipitation and entrainment conditions, Atmospheric Chemistry and Physics, pp. 2729–2746, https://doi.org/10.5194/acp-23-2729-2023, 2023.

Sourdeval, O., Labonnote, L. C., Brogniez, G., Jourdan, O., Pelon, J., and Garnier, A.: A variational approach for retrieving ice cloud properties from infrared measurements: application in the context of two IIR validation campaigns, Atmospheric Chemistry and Physics, https://doi.org/10.5194/acp-13-8229-2013, 2013.

Sourdeval, O., C.-Labonnote, L., Baran, A. J., and Brogniez, G.: A methodology for simultaneous retrieval of ice and liquid water cloud properties. Part I: Information content and case study, Quarterly Journal of the Royal Meteorological Society, https://doi.org/10.1002/qj.2405, 2015.

Stocker, T. F., Qin, D., Plattner, G.-K., Tignor, M. M. B., Allen, S. K., Boschung, J., Nauels, A., Xia, Y., Bex, V., and Midgley, P. M., eds.: Climate change 2013: the physical science basis: Working Group I contribution to the Fifth assessment report of the Intergovernmental Panel on Climate Change, Cambridge University Press, ISBN 9781107057999, 2013.

Trenberth, K. E. and Smith, L.: The Mass of the Atmosphere: A Constraint on Global Analyses, Journal of Climate, pp. 864–875, https://doi.org/10.1175/JCLI-3299.1, 2005.

Vesperini, M., Breon, F.-M., and Tanre, D.: Atmospheric Water Vapor Content from Spaceborne POLDER Measurements, IEEE Transactions on Geoscience and Remote Sensing, https://doi.org/10.1109/36.763275, 1999.

Wyser, K.: The Effective Radius in Ice Clouds, Journal of Climate, pp. 1793–1802, https://doi.org/10.1175/1520-0442(1998)011<1793:TERIIC>2.0.CO;2, 1998.